nature geoscience

SUPPLEMENTARY INFORMATION

https://doi.org/10.1038/s41561-018-0191-8

In the format provided by the authors and unedited.

Increased nutrient supply to the Southern Ocean during the Holocene and its implications for the pre-industrial atmospheric CO_2 rise

Anja S. Studer[1,9]*, Daniel M. Sigman[2], Alfredo Martínez-García[1], Lena M. Thöle[3], Elisabeth Michel[4], Samuel L. Jaccard[3], Jörg A. Lippold[5], Alain Mazaud[4], Xingchen T. Wang[2,6], Laura F. Robinson[7], Jess F. Adkins[6] and Gerald H. Haug[1,8]

[1]Max Planck Institute for Chemistry, Climate Geochemistry Department, Mainz, Germany. [2]Department of Geosciences, Princeton University, Princeton, NJ, USA. [3]Institute of Geological Sciences and Oeschger Center for Climate Change Research, University of Bern, Bern, Switzerland. [4]Laboratoire des Sciences du Climat et de l'Environnement (LSCE), Gif-sur-Yvette, France. [5]Institute of Earth Sciences, Heidelberg University, Heidelberg, Germany. [6]Division of Geological and Planetary Sciences, California Institute of Technology, Pasadena, CA, USA. [7]Bristol Isotope Group, School of Earth Sciences, University of Bristol, Bristol, UK. [8]Department of Earth Sciences, ETH Zurich, Zurich, Switzerland. [9]Present address: Department of Environmental Sciences, University of Basel, Basel, Switzerland. *e-mail: anja.studer@unibas.ch

Supplementary Information to

Increased nutrient supply to the Southern Ocean during the Holocene and its implications for the pre-industrial atmospheric CO_2 rise

Supplementary Information Sections

Supplementary Information 1: Effect of reconstructed changes on atmospheric CO_2 concentration

There are two routes by which the observed increase in surface nutrients and enhanced overturning in the Southern Ocean over the Holocene may have raised atmospheric CO_2, involving respectively the upper and lower overturning cells of the Southern Ocean. The upper cell effect is similar to that described in association with changes in Subantarctic iron fertilization[14]. Over the course of the Holocene, the rise in surface nutrient concentrations would imply (1) an increase in ocean preformed (unused) nutrients, (2) a transfer of remineralized CO_2 from the deep ocean to the atmosphere, causing precipitation of deep sea calcium carbonate, which lowers ocean alkalinity and raises atmospheric CO_2 by a second mechanism, and (3) nutrient leakage to the low latitudes, increasing $CaCO_3$ productivity and flux to the seabed, thus lowering ocean alkalinity and raising atmospheric CO_2 by this third mechanism[38]. The lower cell effect was the first one described[8,60,61] and would raise atmospheric CO_2 concentrations through both (1) increasing the amount of preformed nutrients returning into the deep ocean and (2) increasing the importance of the AZ in ventilating the ocean interior. The lower cell effect is the focus of the experiments of the study of Hain *et al.*[38] to estimate the possible lower cell impact on CO_2. Assuming from the observed $\delta^{15}N_{db}$ change that the surface nitrate concentration increase over the Holocene was roughly half of the total rise since the Last Glacial Maximum[15], the effects on atmospheric CO_2 are ~15-20 ppm from both the upper cell[62] and lower cell[38]. If both were activated, the CO_2 effect could have been as much as 40 ppm, that is, greater than the observed change. However, lacking data from the more polar AZ, we cannot say whether the lower cell component was partially or fully activated.

Supplementary Information 2: Diatom separation and cleaning protocol

This protocol is suitable to extract the diatom opal from most Southern Ocean sediments. Depending on the diatom species composition, sieve mesh size and settling time may need to be adjusted.

Physical separation of diatom opal from bulk sediment

1. Place ~2 g freeze-dried sediment in centrifuge tube (50 mL conical-bottom, polypropylene)
2. Add ~40 mL of 2% sodiumpolyphosphate (Na-poly-PO_4) solution, vortex
3. Sieve off >63 µm fraction, keeping the <63µm fraction
4. Pour sample into standard 200 mL beaker, fill with Na-poly-PO_4 to 200 mL mark
5. Allow to settle 1.5 hours (maybe longer, depending on diatom species composition), then pour off supernatant
6. Repeat steps 4 and 5 with H_2O until liquid overlying sediment appears clear
7. Wash samples back into centrifuge tubes; centrifuge (20 minutes at 4000 rpm) and pour off liquid
8. Remove carbonate with 3:1 H_2O:HCl, wash samples with H_2O until pH is neutral
9. Dry sediments in oven overnight at 60°C (not completely dry)
10. Add 40 mL of sodium-polytungstate (SPT) diluted to a density of 2.15 g/cm^3
11. Vortex and centrifuge for 20 minutes at 4000 rpm
12. Slightly agitate centrifuge tube and decant supernatant and SPT into a new, clean centrifuge tube, leaving behind sedimented bottom layer
13. Repeat steps 11 and 12 until there is no sedimented fraction
14. Pour supernatant and SPT through 8.0 µm polycarbonate filter. Recycle SPT.
15. Rinse filter and sample with 500 mL of H_2O
16. Cut filter in 3 pieces: keep ¼ uncleaned aliquot for reserve, ¼ for total diatom analysis, ½ for pennate-centric separation. Place subsamples in clean centrifuge tubes
17. Add 40 mL of H_2O to each subsample; vortex and remove filter. Centrifuge and pour off water

18. With total diatom sample, proceed with chemical cleaning (below). For pennate-centric separation, follow cartoon in figure 3 of Studer *et al.*[15]. In addition, after pennate-centric separation, rinse centric fraction over a 20µm sieve. Wash back into centrifuge tube.

Chemical cleaning of diatom opal

1. Add ~15 mL dithionite-citric acid to sample, vortex
   [*Dithionite-citric acid:* Stock solution: 500 mL H_2O + 31 g Sodium Citrate ($Na_3C_6H_5O_7$*$2H_2O$) + 5 g Sodium Bicarbonate ($NaHCO_3$)
   Working solution: Add 0.5 g Sodium Dithionite ($Na_2S_2O_4$) per 10 mL of stock solution]
2. Let sit for 1 hour in 80°C water bath
3. Dilute solution with H_2O to 40 mL; centrifuge and pour-off
4. Rinse samples with another 40 mL of H_2O, centrifuge and pour off
5. Add ~25 mL diluted perchloric acid (9 parts H_2O, 1 part concentrated ~ 70% perchloric acid) to sample and cap loosely
6. Place samples in boiling water bath for 1 hour
7. Let samples cool, then centrifuge and decant
8. Transfer samples to 40 mL glass tubes
9. Add ~20 mL 70% perchloric acid and cap tightly (with PTFE lined caps)
10. Let samples sit for ~2 hours (only if samples are rich in organics)
11. Loosen caps to allow release of evolved gas and then retighten (only if samples are rich in organics)
12. Place samples in boiling water bath for 2 hours
13. Let samples cool, then pour off most of the perchloric acid
14. Wash samples back into cleaned centrifuge tubes, and dilute with H_2O to 40 mL mark. Centrifuge, decant.
15. Rinse (i.e., vortex, centrifuge, decant) at least three times with 40 mL H_2O (until pH neutral)
16. After final pour-off, place in clean (vacuum-)oven overnight
17. Transfer dry samples to combusted glass vials with acid washed snap-caps.

Supplementary Figures

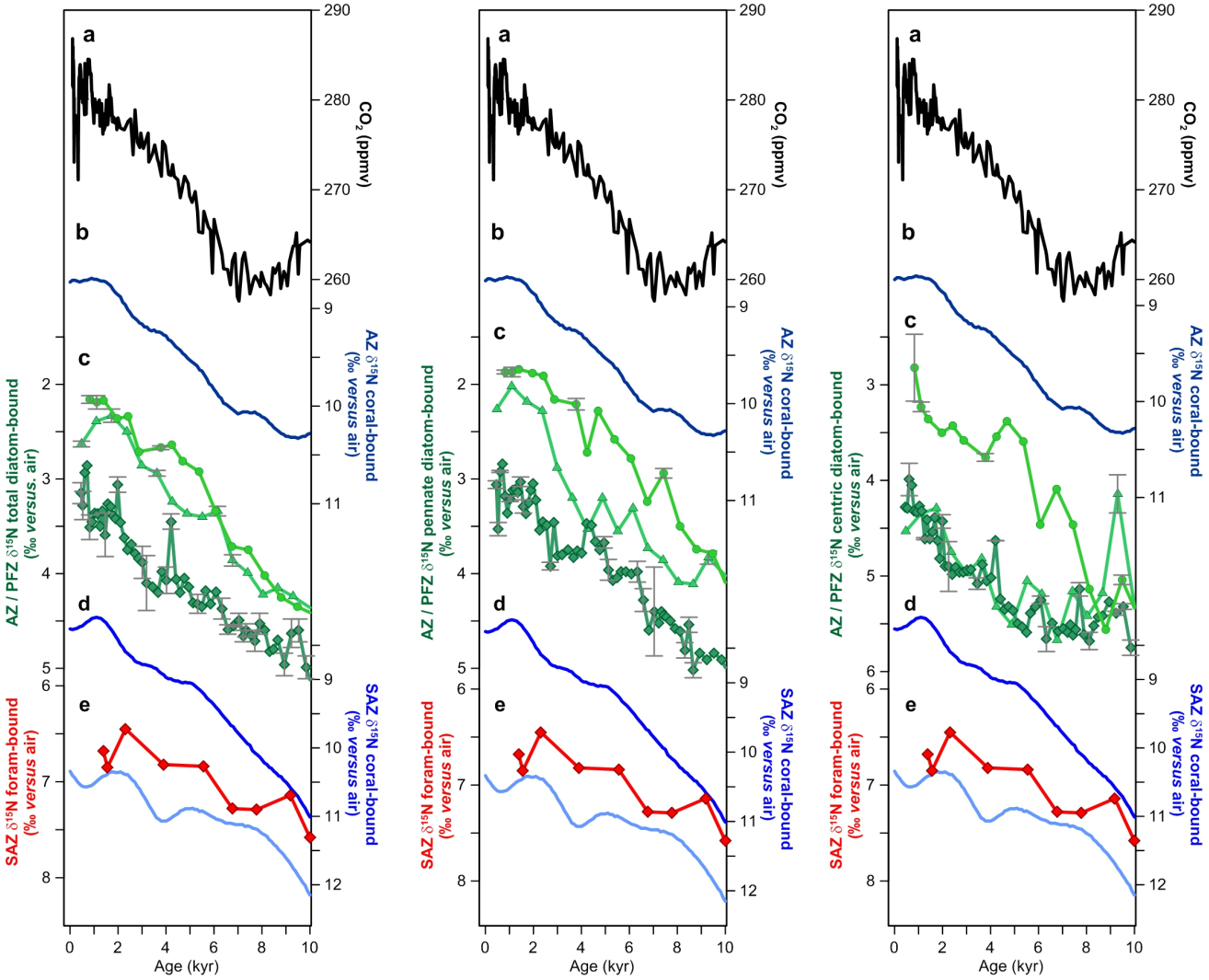

MD12-3396CQ, separated diatom opal, Holocene (1cm core depth)

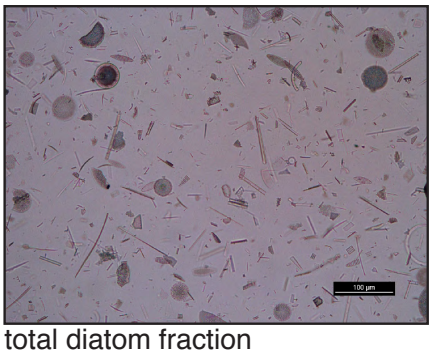
total diatom fraction

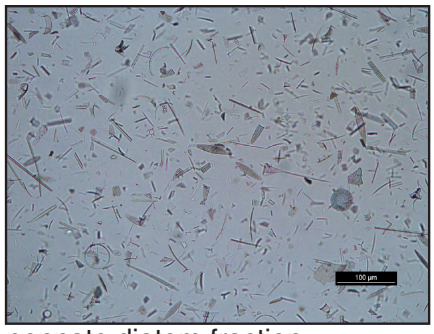
pennate diatom fraction

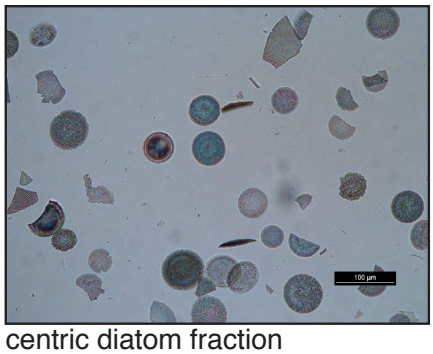
centric diatom fraction

Supplementary Figure S1.

***Top*: Holocene compilation of fossil-bound $\delta^{15}N$ records alongside atmospheric CO_2.** Changing among the three upper panels is the diatom-bound $\delta^{15}N$ data (green), with the $\delta^{15}N_{db}$ of the total diatom fraction shown on the left, the $\delta^{15}N_{db}$ of the pennate diatom fraction shown in the middle, and the $\delta^{15}N_{db}$ of the centric diatom fraction shown on the right (see bottom panel for visual examples). **a,** Atmospheric CO_2 concentration composite[52]. **b,** Compilation of AZ coral-bound $\delta^{15}N$ data[16] (Drake Passage). **c,** Diatom-bound $\delta^{15}N$ from the Pacific Antarctic[15] (circles, PS75/72-4), the Indian Antarctic (triangles, MD11-3353) and the Indian Polar Frontal Zone (diamonds, MD12-3396CQ). Error bars indicate the standard deviation of replicate measurements. **d,** Coral-bound $\delta^{15}N$ records from the Subantarctic Zone of the Southern Ocean[16] (dark-blue, Drake Passage, light-blue, south of Tasmania). **e,** Foraminifera-bound $\delta^{15}N$ record from ODP 1090 in the SAZ Atlantic[14]. Data in **a** is shown for the period prior to 1900. Note that the right-hand axis in **d** (SAZ $\delta^{15}N$ coral-bound) has been scaled by two-thirds for plotting purposes.

***Bottom:* Photomicrograph examples of the different separated diatom opal fractions.** Shown is a Holocene diatom opal sample from sediment core MD12-3396CQ that was separated into the total diatom fraction (left), pennate diatom fraction (middle) and centric diatom fraction (right), according to the protocols described in Supplementary Information Section S2 and figure 3 of Studer *et al.*[15]. Scale bars are 100 µm.

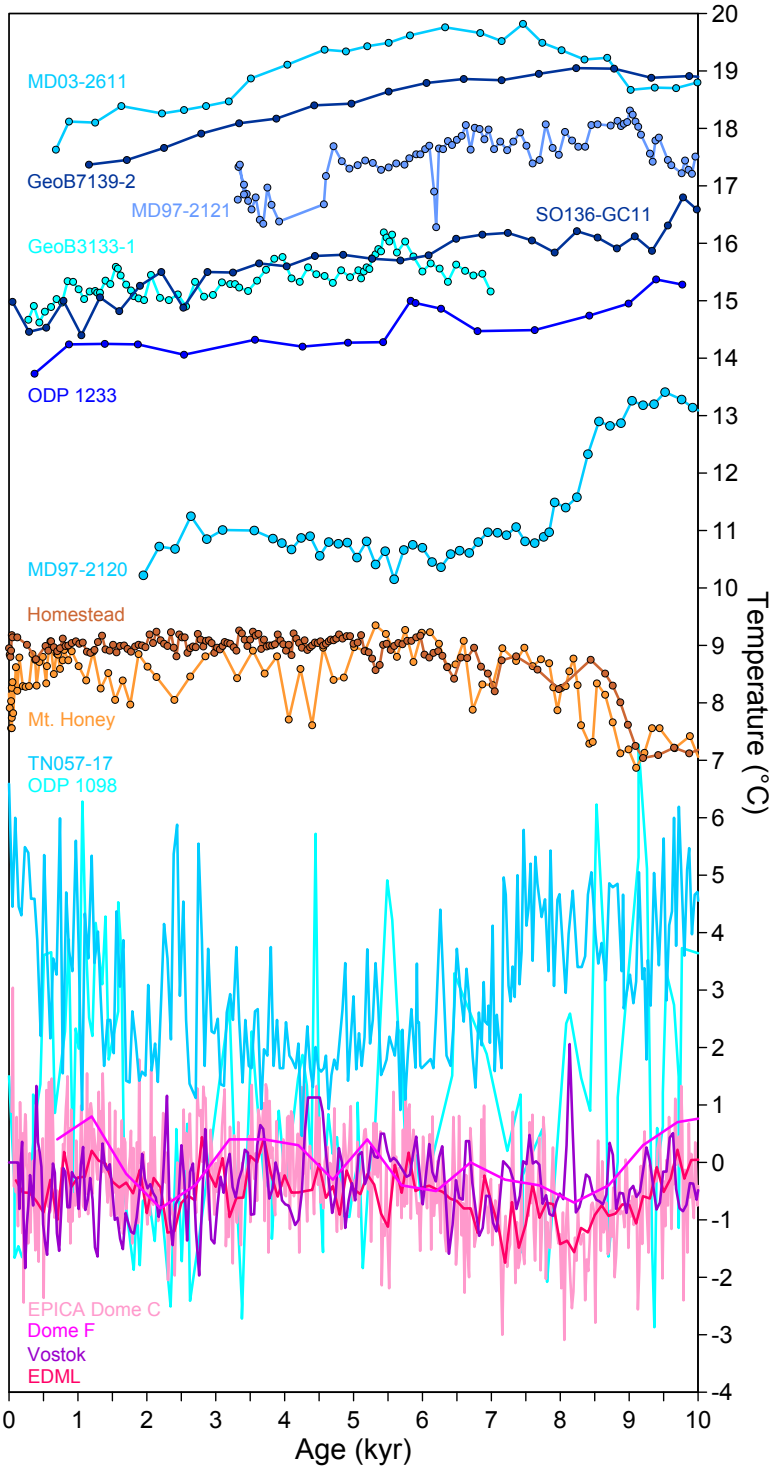

Supplementary Figure S2. Compilation of proxy records showing atmospheric and oceanic temperature changes in the Southern Hemisphere across the Holocene time period as given in Supplementary Table S2. Oceanic SSTs are cooling throughout the Holocene, while most atmospheric temperature records indicate warming. See Supplementary Figure S6 for the location of these records on a map, and Supplementary Table S2 for references.

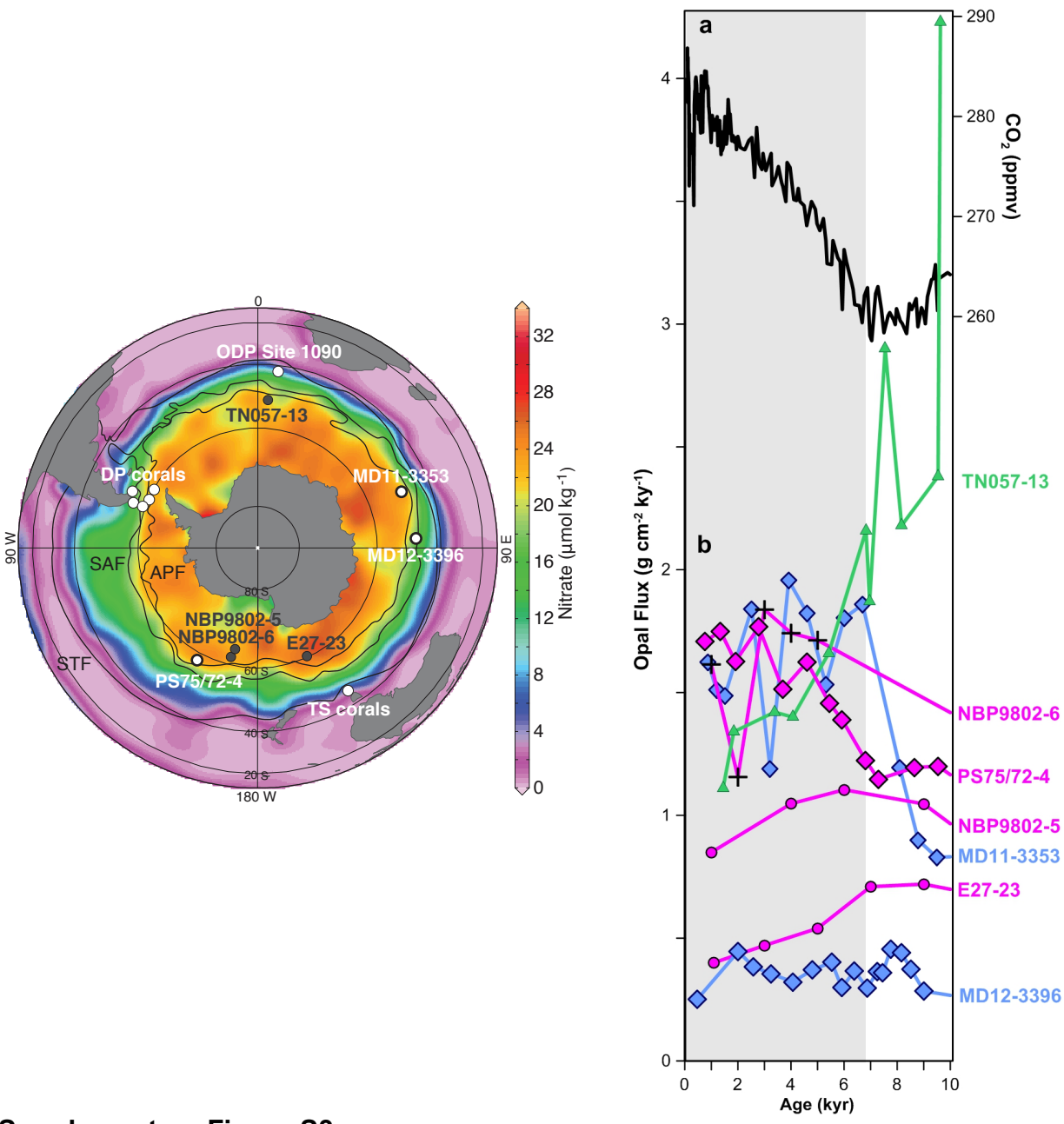

Supplementary Figure S3.

Left: **Sediment core and deep sea coral locations as shown in figure 1 including locations of opal flux records shown on the right.**

Right: **Compilation of opal flux records alongside atmospheric CO_2. a,** Atmospheric CO_2 concentration composite[52]. **b,** Compilation of opal flux records from the Indian (blue), Pacific (pink) and Atlantic (green) sectors of the Southern Ocean[11,15,63]. Although more opal flux records exist in the literature we have only included in the compilation those that have radiocarbon constraints for the Holocene and at least 3 data points in the late Holocene (0-6 kyrs), so that potential dating uncertainties are minimized and observed trends can be considered reliable.

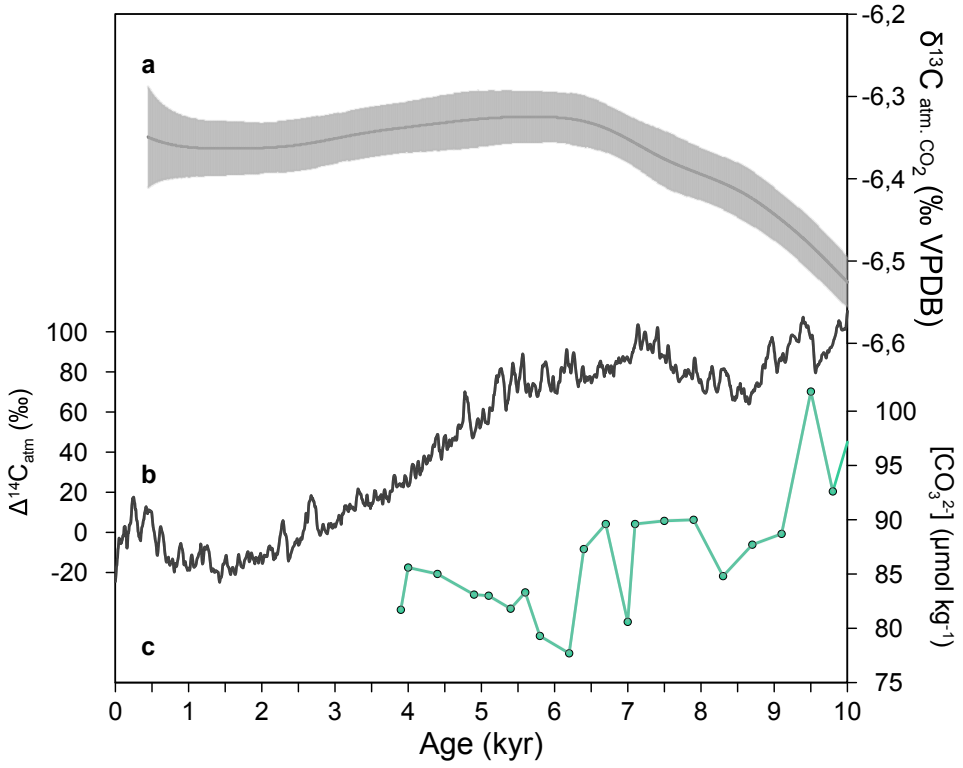

Supplementary Figure S4. Compilation of carbon cycle-related data discussed in the main text. **a**, Carbon isotopic composition of atmospheric CO_2 (ref. 39). **b**, Holocene evolution of atmospheric $\Delta^{14}C$ from IntCal13 (ref. 64). **c**, Reconstructed deep sea carbonate ion concentration of the deep Indian Ocean[41]. For the compilation of benthic foraminiferal $\delta^{13}C$ records, see ref. 43 (Figure D1, panel c).

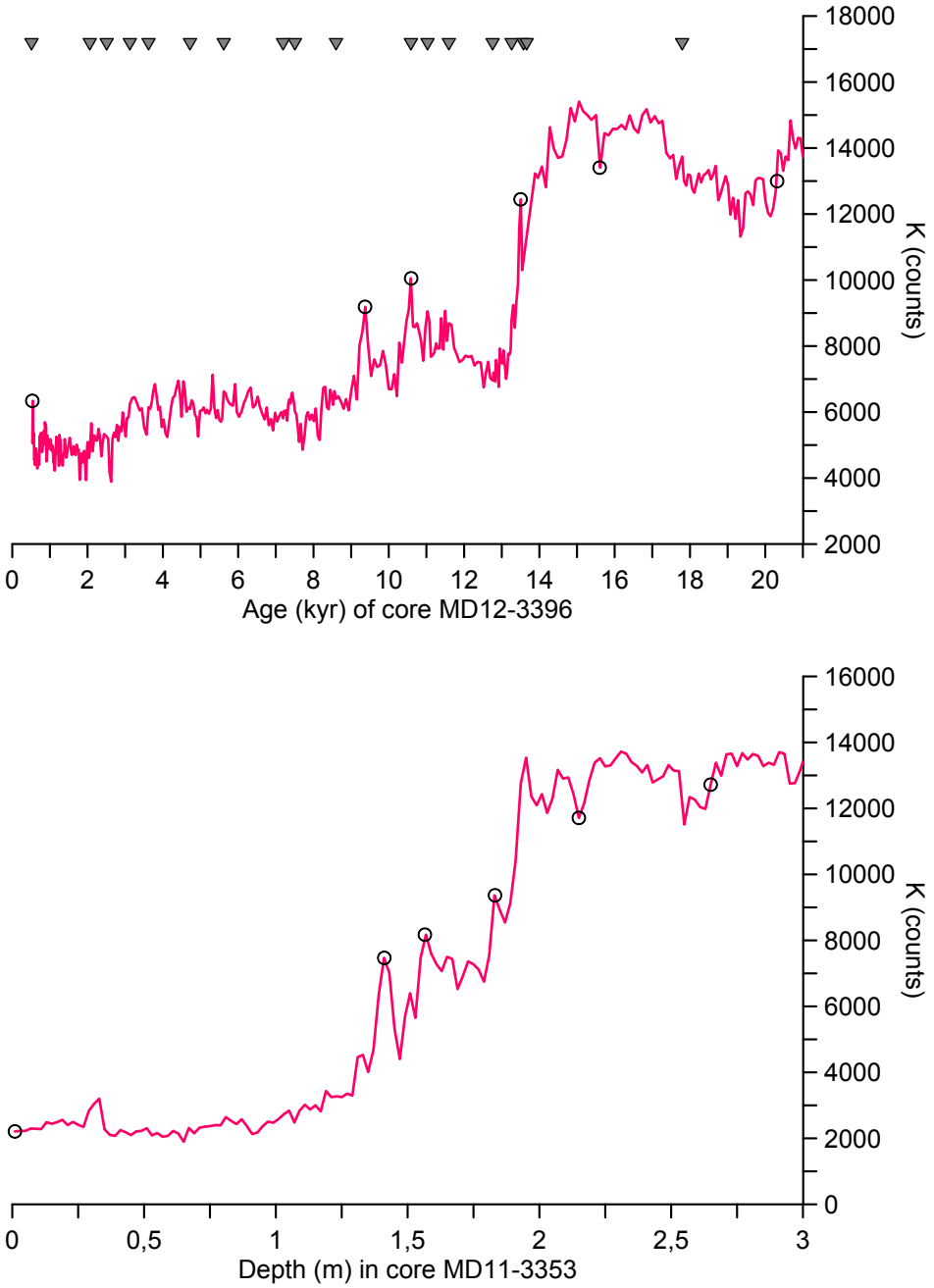

Supplementary Figure S5. Construction of age model for core MD11-3353. Distinctive features in the potassium (K) XRF scanning record of MD11-3353 were correlated to those in MD12-3396CQ (black circles). The core-top of MD11-3353 was assigned the same age than the core-top of MD12-3396CQ to allow for the possibility that the sediment surface was lost during coring. The triangles in the upper panel denote the radiocarbon ages of core MD12-3396CQ.

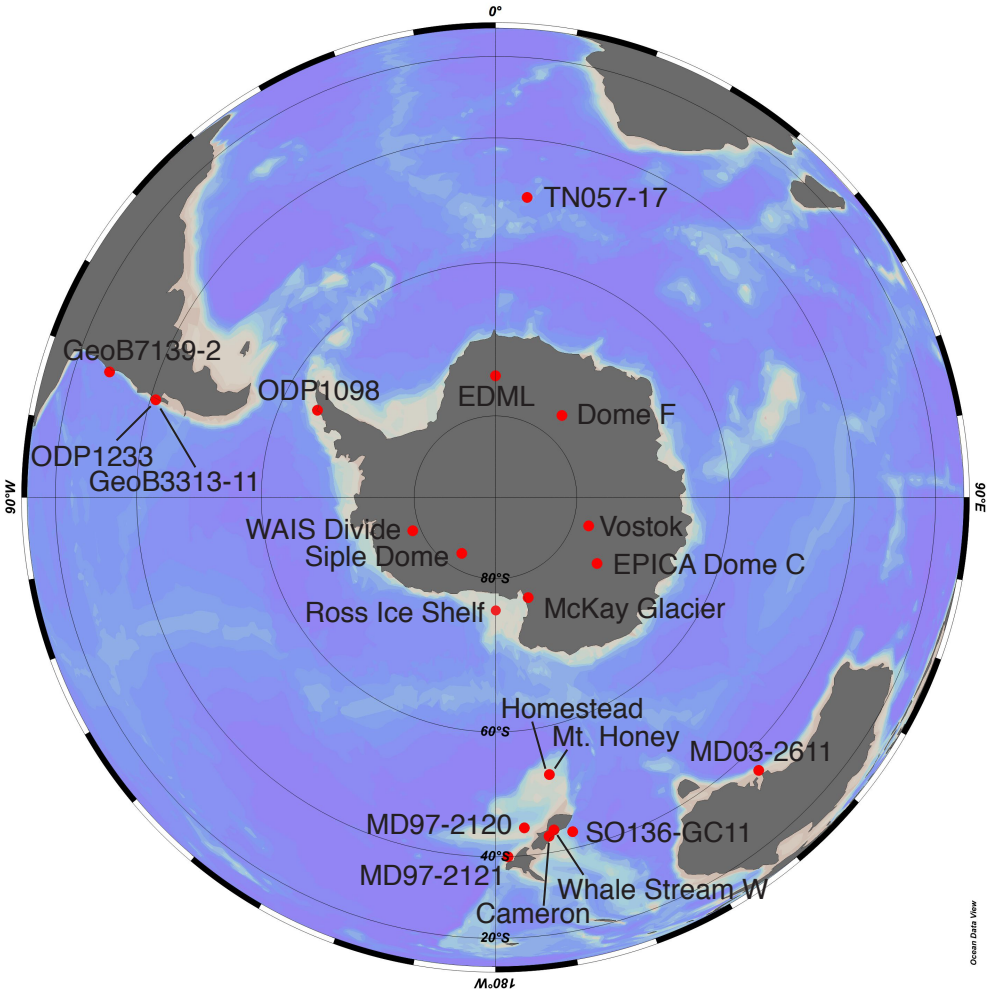

Supplementary Figure S6. Location of temperature record sites given in Supplementary Figure S2 and Supplementary Table S2.

Supplementary Tables

Supplementary Table S1

Radiocarbon ages measured on sediment core MD12-3396CQ. The ^{14}C ages were converted to calendar ages using calibration curve SH2013 and a marine reservoir age of 900±100 years.

Lab code	Foraminifera species	core depth (cm)	conventional ^{14}C age (yr)	mean conventional ^{14}C age (yr)	calendar age (yr BP)		
					median	upper limit	lower limit
SacA39690	*G. bulloides*	4	1445 ± 30	1445 ± 10	510	432	622
SacA39704	*G. inflata*	4	1445 ± 30				
SacA39705	*G. inflata*	64	2965 ± 30	2965 ± 30	2059	1924	2182
SacA39691	*G. bulloides*	76	3365 ± 30	3365 ± 30	2506	2375	2625
SacA39692	*G. bulloides*	92	3860 ± 30	3860 ± 30	3123	2992	3256
SacA39707	*G. inflata*	100	4345 ± 30	4345 ± 30	3623	3495	3741
SacA39693	*G. bulloides*	124	5050 ± 30	5135 ± 120	4718	4523	4901
SacA40482	*N. Pachyderma sin.*	124	5220 ± 50				
SacA39694	*G. bulloides*	144	5810 ± 35	5810 ± 35	5616	5488	5746
SacA40483	*N. Pachyderma sin.*	172	7270 ± 90	7270 ± 90	7191	7065	7341
SacA39695	*G. bulloides*	184	7550 ± 35	7547.5 ± 10	7510	7435	7589
SacA39708	*G. inflata*	184	7545 ± 35				
SacA39696	*G. bulloides*	208	8660 ± 40	8705 ± 65	8596	8403	8725
SacA40484	*N. Pachyderma sin.*	208	8750 ± 90				
SacA40485	*N. Pachyderma sin.*	236	10300 ± 80	10300 ± 80	10590	10400	10762
SacA39709	*G. inflata*	244	10655 ± 50	10655 ± 50	11031	10882	11198

Supplementary Table S2

Compilation of available proxy records addressing atmospheric and oceanic temperature changes in the Southern Hemisphere across the Holocene time period. See Supplementary Figure S2 for a graphic version of the records (note that not all of the records listed below are available or suitable for plotting). See Supplementary Figure S6 for the location of these records on a map.

Core / Site name	Realm	Latitude	Longitude	Proxy	Reference	Holocene Temperature trend
MD97-2120	marine	45° S	175° E	alkenone SST	Pahnke and Sachs, 2006 (ref. 65)	4°C cooling from 11-7ka, no change 7-0 ka
MD97-2121	marine	40° S	178° E	alkenone SST	Pahnke and Sachs, 2006 (ref. 65)	2°C cooling from 9-3 ka
ODP 1233	marine	41° S	74° W	alkenone SST	Kaiser et al., 2005 (ref. 66)	2°C cooling from 10-0 ka
GeoB7139-2	marine	30° S	72° W	alkenone SST	Kaiser et al., 2008 (ref. 67)	1.5°C cooling from 9-1 ka
MD03-2611	marine	36° S	136° E	alkenone SST	Calvo et al., 2007 (ref. 68)	2°C cooling from 6.5-0 ka
ODP 1098	marine	65° S	64° W	TEX_{86} SST	Shevenell et al., 2011 (ref. 69)	3-4°C cooling from 12-0 ka
SO136-GC11	marine	43° S	167° E	alkenone SST	Barrows et al., 2007 (ref. 70)	2°C cooling from 10-0 ka
GeoB3313-1	marine	41° S	74° W	alkenone SST	Lamy et al., 2002 (ref. 71)	0.8°C warming from 7-5.5 ka, 1.5°C cooling from 5.5-0 ka
TN057-17	marine	50° S	6° E	diatom MAT	Nielsen et al., 2004 (ref. 72)	3°C cooling from 10-5 ka, 3°C warming 4-0 ka
Homestead	terrestrial	53° S	169° E	pollen MAT	McGlone et al., 2010 (ref. 73)	2°C warming 10-6 ka, no change 6-0 ka
Mt. Honey	terrestrial	53° S	169° E	pollen MAT	McGlone et al., 2010 (ref. 73)	2°C warming 10-6 ka, 1°C cooling 6-4 ka, no change 4-0 ka
Cameron	mountain glacier	43° S	171° E	^{10}Be exposure age	Putnam et al., 2012 (ref. 74)	mountain glacier recession from 11-3 ka
Whale Stream W	mountain glacier	44° S	170° E	^{10}Be exposure age	Kaplan et al., 2013 (ref. 75)	mountain glacier recession from 11-0 ka
McKay Glacier	EAIS outlet glacier	77° S	162° E	^{10}Be exposure age sediment	Jones et al., 2015 (ref. 76)	EAIS outlet glacier rapidly thinned around 7ka
Ross Ice Shelf	Ice Shelf	74-78° S	170° W - 170° E	composition, ^{10}Be concentration in sediment underlying ice shelf	Yokoyama et al., 2016 (ref. 77)	Ross Ice Shelf collapse from 5-1.5 ka
EPICA Dome C	ice core	75° S	123° E	δD	Jouzel et al., 2007 (ref. 78)	1.5°C cooling 10-8 ka, 1.5°C warming 8-6 ka, no change 6-0 ka
Dome F	ice core	77° S	39° E	$\delta^{18}O$, δD	Kawamura et al., 2007 (ref. 79)	noisy, no clear trend
Vostok	ice core	78° S	107° E	δD	Petit et al., 1999 (ref. 80)	no change over the last 11 ka
EDML	ice core	75° S	0° E	$\delta^{18}O$	Stenni et al., 2011 (ref. 81)	1.5°C cooling 10-8 ka, 1°C warming 8-0 ka
WAIS Divide	ice core	79° S	112° W	δD	Buizert et al., 2015 (ref. 82)	1°C warming 10-4 ka, 1°C cooling 4-0 ka
Siple Dome	ice core	82° S	149° W	melt layers	Das and Alley, 2008 (ref. 83)	incresing melt layer frequency from 6.6-0 ka

Supplementary Data files

The new data presented in this manuscript will be archived at Pangaea at https://doi.pangaea.de/10.1594/PANGAEA.891436 and is available in the Supplementary Information.

Supplementary References

(60) Siegenthaler, U. & Wenk, Th. Rapid atmospheric CO_2 variations and ocean circulation. *Nature* **308,** 624-626 (1984).

(61) Knox, F. & McElroy, M. B. Changes in atmospheric CO_2: Influence of the marine biota at high latitude. *J. Geophys. Res.* **89,** 4629-4637 (1984).

(62) Robinson, R. S. et al. Diatom-bound $^{15}N/^{14}N$: New support for enhanced nutrient consumption in the ice age Subantarctic. *Paleoceanography* **20,** PA3003 (2005).

(63) Chase, Z., Anderson, R. F., Fleisher, M. Q. & Kubik, P. W. Accumulation of biogenic and lithogenic material in the Pacific sector of the Southern Ocean during the past 40,000 years. *Deep-Sea Res. II* **50,** 799-832 (2003).

(64) Reimer, P. J. et al. IntCal13 and Marine13 radiocarbon age calibration curves 0-50'000 years cal BP. *Radiocarbon* **55,** 1869-1887 (2013).

(65) Pahnke, K. & Sachs, J. P. Sea surface temperatures of southern midlatitudes 0-160 kyr B.P. *Paleoceanography* **21,** PA2003 (2006).

(66) Kaiser, J., Lamy, F. & Hebbeln, D. A 70-kyr sea surface temperature record off southern Chile (Ocean Drilling Program Site 1233). *Paleoceanography* **20,** PA4009 (2005).

(67) Kaiser, J., Schefuss, E., Lamy, F., Mohtadi, M. & Hebbeln, D. Glacial to Holocene changes in sea surface temperature and coastal vegetation in north central Chile: high versus low latitude forcing. *Quat. Sci. Rev*. **27,** 2064-2075 (2008).

(68) Calvo, E., Pelejero, C., De Deckker, P. & Logan, G. A. Antarctic deglacial pattern in a 30 kyr record of sea surface temperature offshore South Australia. *Geophys. Res. Lett*. **34,** L13707 (2007).

(69) Shevenell, A. E., Ingalls, A. E., Domack, E. W. & Kelly, C. Holocene Southern Ocean surface temperature variability west of the Antarctic Peninsula. *Nature* **470,** 250-254 (2011).

(70) Barrows, T. T., Lehman, S. J., Fifield, L. K. & De Deckker, P. Absence of cooling in New Zealand and the adjacent ocean during the Younger Dryas chronozone. *Science* **318,** 86-89 (2007).

(71) Lamy, F., Rühlemann, C., Hebbeln, D. & Wefer, G. High- and low-latitude climate control on the position of the southern Peru-Chile current during the Holocene. *Paleoceanography* **17 (2),** 1028 (2002).

(72) Nielsen, S. H. H., Koç, N. & Crosta, X. Holocene climate in the Atlantic sector of the Southern Ocean: controlled by insolation or oceanic circulation? *Geology* **32,** 317-320

(2004).

(73) McGlone, M. S., Turney, C. S. M., Wilmshurst, J. M., Renwick, J. & Pahnke, K. Divergent trends in land and ocean temperature in the Southern Ocean over the past 18,000 years. *Nat. Geosci.* ***3,*** 622-626 (2010).

(74) Putnam, A. E. et al. Regional climate control of glaciers in New Zealand and Europe during the pre-industrial Holocene. *Nat. Geosci.* **5,** 627-630 (2012).

(75) Kaplan, M. R. et al. The anatomy of long-term warming since 15 ka in New Zealand based on net glacier snowline rise. *Geology* **41,** 887-890 (2013).

(76) Jones, R. S. et al. Rapid Holocene thinning of an East Antarctic outlet glacier driven by marine ice sheet instability. *Nat. commun*. **6,** 8910 (2015).

(77) Yokoyama, Y. et al. Widespread collapse of the Ross Ice Shelf during the late Holocene. *Proc. Natl. Acad. Sci. USA* **9,** 2354-2359 (2016).

(78) Jouzel, J. et al. Orbital and millennial Antarctic climate variability over the past 800,000 years. *Science* **317,** 793-796 (2007).

(79) Kawamura, K. et al. Northern Hemisphere forcing of climate cycles in Antarctica over the past 360,000 years. *Nature* **448,** 912-916 (2007).

(80) Petit, J. R. et al. Climate and atmospheric history of the past 420,000 years from the Vostok ice core, Antarctica. *Nature* **399,** 429-436 (1999).

(81) Stenni, B. et al. Expression of the bipolar see-saw in Antarctic climate records during the last deglaciation. *Nat. Geosci.* **4,** 46-49 (2011).

(82) Buizert, C. et al. The WAIS Divide deep ice core WD2014 chronology – Part 1: Methane synchronization (68-31 ka BP) and the gas age-ice age difference. *Clim. Past* **11,** 153-173 (2015).

(83) Das, S. B. & Alley, R. B. Rise in frequency of surface melting at Siple Dome through the Holocene: Evidence for increasing marine influence on the climate of West Antarctica. *J. Geophs. Res. – Atmos.* **113,** D02112 (2008).